ACS APPLIED MATERIALS & INTERFACES

Research Article

Cite This: ACS Appl. Mater. Interfaces 2018, 10, 15461−15466

www.acsami.org

# Reversing Multidrug Resistance by Multiplexed Gene Silencing for Enhanced Breast Cancer Chemotherapy

Yanli Li,[†] Xiaonan Gao,[†] Zhengze Yu, Bo Liu, Wei Pan, Na Li,* and Bo Tang*

College of Chemistry, Chemical Engineering and Materials Science, Collaborative Innovation Center of Functionalized Probes for Chemical Imaging in Universities of Shandong, Key Laboratory of Molecular and Nano Probes, Ministry of Education, Institute of Molecular and Nano Science, Shandong Normal University, Jinan 250014, P. R. China

Supporting Information

**ABSTRACT:** Multidrug resistance (MDR), as one of the main problems in clinical breast cancer chemotherapy, is closely related with the over expression of drug efflux transporter P-glycoprotein (P-gp). In this study, a novel drug-loaded nanosystem was developed for inhibiting the P-gp expression and reversing MDR by multiplexed gene silencing, which composes of graphene oxide (GO) modified with two molecular beacons (MBs) and Doxorubicin (Dox). When the nanosystem was uptaken by the MDR breast cancer cells, Dox was released in the acidic endosomes and MBs were hybridized with target sequences. The intracellular multidrug resistance 1 (MDR1) mRNA and upstream erythroblastosis virus E26 oncogene homolog 1 (ETS1) mRNA can be silenced by MBs, which can effectively inhibit the expression of P-gp and further prevent the efflux of Dox and reverse MDR. In vitro and in vivo studies indicated that the strategy of reversing MDR by multiplexed gene silencing could obviously increase MCF-7/Adr cells' Dox accumulation and enormously enhance the therapeutic efficacy of MDR breast cancer chemotherapy.

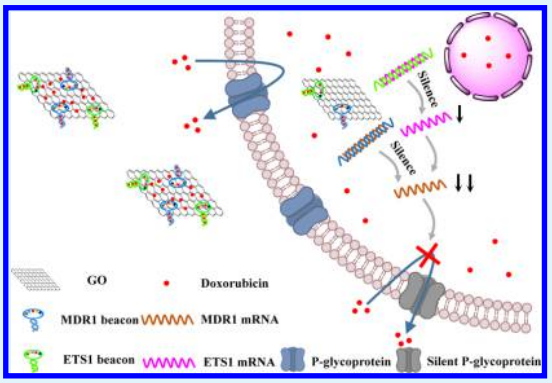


**KEYWORDS:** *multidrug resistance, multiplexed gene silencing, graphene oxide, molecular beacon, P-glycoprotein*

## INTRODUCTION

Breast cancer, a threat to women's health, is a malignant tumor and the main cause of cancer death.[1] Chemotherapy as one of the major therapeutic methods, however, still faces the multidrug resistance (MDR) problem that seriously disturbs the efficacy or even leads to failure.[2] Therefore, effectively solving the problem of breast cancer MDR becomes one of the biggest challenges in clinical applications. According to the American Cancer Society, over 90% of cancer patients died of varying degrees of MDR in all types of cancers.[3] MDR refers to the cancer cells' resistance toward the drugs that are used in chemotherapy, as well as other structurally and mechanistically unrelated drugs that exhibit cross-resistance.[4] However, among many causes and factors of MDR, over expression of P-glycoprotein (P-gp) plays a significant role by encoding the multidrug resistance 1 (MDR1) for drugs' interception and exportation before reaching their intracellular targets.[5] Consequently, exploring efficient ways to solve the problem and improve the cancers' cure rate has been the hot spot of the current cancer research.

Aiming at the cancer MDR, the traditional methods took advantage of increasing the loading amount of drugs on the nanocarriers to destroy MDR cancer cells.[6] However, because of the high toxicity and side effects of anticancer drugs toward normal cells and tissues, the large doses of the drug application have been strictly limited. In this regard, most studies have been focused on utilizing MDR1 siRNA to inhibit the expression of efflux transporter P-gp and then handling MDR tumor combined with chemotherapy drugs.[7,8] Nevertheless, because of the high price and easy degradability of siRNA, drugs with directional accumulation and slow releasing functionalities have been prepared recently for the method of integrating photothermal and photodynamic therapy with chemotherapy[9,10] or the drug "transformation" approach.[11] Even though such methods are mainly palliatives, they do not solve the problem of MDR from the essence of the cell signaling pathways and signal transduction. Therefore, developing a more economic, safe, and effective method to essentially solve the MDR problem is highly desirable for enhancing the cancer therapeutic effect.

Herein, we report a novel drug-loaded nanosystem for reversing MDR in breast cancer. In this study, graphene oxide (GO) was chosen as carrier to absorb Doxorubicin (Dox) and Dox-embedded molecular beacons (MBs) via $\pi-\pi$ stacking interactions.[12] MBs are stem-loop-structured antisense oligonucleotides and are widely used for detection and imaging of molecular targets in living cells.[13,14] Moreover, as the loop sequences of MBs specifically hybridize with the target mRNAs,

Received: February 14, 2018
Accepted: April 17, 2018
Published: April 17, 2018




DOI: 10.1021/acsami.8b02800
ACS Appl. Mater. Interfaces 2018, 10, 15461−15466

MBs are adopted as promising tools for gene silencing.[15−18] The MDR1 gene can encode P-gp which can transport Dox,[19] and the erythroblastosis virus E26 oncogene homolog 1 (ETS1) gene as the upstream of MDR1 can positively regulate the expression of MDR1.[20−23] When the nanosystem was internalized into MCF-7/Adr cells, the release of Dox was promoted in the acidic endosomes, and the MBs were hybridized with target sequences. Accordingly, MDR1 mRNA and upstream ETS1 mRNA were simultaneously silenced by MBs, which suppress the expression of P-gp and inhibit the Dox efflux (Scheme 1). The synergistic effect could tremendously enhance the therapeutic efficacy of chemotherapy for breast cancer.

**Scheme 1. Schematic Illustration of Drug-Loaded Nanosystems for the Treatment of Multidrug-Resistant Breast Cancer**

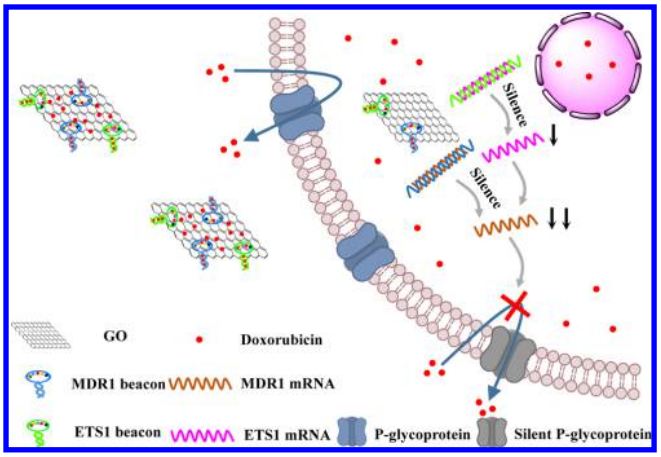


## EXPERIMENTAL SECTION

**Materials.** GO was obtained from Nanjing XFNANO Materials Tech Co., Ltd. Sangon Biotechnology (Shanghai) supplied Doxorubicin hydrochloride (Dox). Triethanolamine (TEA), magnesium chloride hexahydrate ($MgCl_2·6H_2O$), potassium chloride (KCl), and sodium chloride (NaCl) were acquired from Sinopharm (Shanghai). Thiazolyl blue tetrazolium bromide (MTT) was purchased from Sigma-Aldrich. Deoxyribonuclease I (DNase I) was procured from Beijing Solarbio Science & Technology Co., Ltd. All the reagents were analytical grade and used as received. Ultrapure water (18.2 MΩ·cm$^2$) was used in all experiments. Shanghai Sangon Biotechnology and Beijing SBS Genetech supplied the DNA oligonucleotides. Table S1 shows the DNA oligonucleotides' sequences. Anti-P glycoprotein antibody, anti-ETS1 antibody, and secondary antibody (Alexa Fluor 647) were acquired from Abcam (Germany). Beta actin polyclonal antibody was purchased from Proteintech (U. S.).

**Characterization.** The JEM-2100 electron microscope was used to acquire the high-resolution transmission electron microscopy (HRTEM) images. UV−visible absorption spectra were obtained on a UV-1700 UV−vis spectrophotometer (Shimadzu). The FLS-980 Edinburgh fluorescence spectrometer was used to measure the fluorescence spectra. A pH-3c digital pH-meter was used for pH tests. Particle size distribution was performed on Malvern Zetasizer Nano-ZS90. Reverse transcription-polymerase chain reaction (RT-PCR) was carried out on a LineGene 9620 sequence detection system (Bioer, China). The UV absorbance of formazan in MTT assay was carried out on a microplate reader. Confocal imaging studies were carried out using TCS SP5 (Leica) laser scanning confocal microscopy. Flow cytometry was performed with an ImageStream X Mark II imaging flow cytometer (Merck Millipore, USA).

**Quantitation of GO.** To facilitate the research of the chemical system, MDR1 MB and ETS1 MB are labeled as Quasar 670 and FAM, respectively. When the two MBs were 250 nM each, the amount of GO was quantitated according to the fluorescence of the three dyes quenched by GO.

**Preparation of the (MDR1 + ETS1)/Dox−GO [(M + E)/Dox−GO] Nanosystem.** Dox (10 mg) was first dissolved in the mixture solution of dimethylsulphoxide (2 mL) and TEA (6 μL) and then stirred under dark conditions for 12 h to remove hydrochloride. Equimolar of MBs was mixed in Tris-HCl buffer (20 mM, pH 7.4, containing 100 mM NaCl, 5 mM $MgCl_2$, and 5 mM KCl) and then added to GO (82 μg/mL) with a final concentration of 250 nM each. Subsequently, TEA-treated Dox (82 μg/mL) was added to the mixed solution and stirred overnight under dark at room temperature. The mixture was purified through centrifugation at 8000 rpm for 20 min, and the precipitate was dispersed in ultrapure water to obtain the product.

**Hybridization, Kinetic, and Specificity Study.** For the hybridization experiment in a concentration-dependent manner, the nanosystem was diluted in the abovementioned Tris-HCl buffer to 16.4 μg/mL and added to MDR1 targets and ETS1 targets through increasing concentrations of the DNA targets (0, 30, 50, 100, 150, 200, 250, 300, 400, 500, and 1000 nM). After incubation at 37 °C for 0.5 h, the fluorescence intensities of Quasar 670 and FAM with excitations at 648 and 492 nm, respectively, were measured.

The nanosystem (16.4 μg/mL) was incubated with the perfectly matched DNA target (400 nM) at 37 °C with different incubation times (0, 5, 10, 15, 20, 30, 40, 50, and 60 min). In addition, the control group of another nanosystem portion was incubated without the DNA target, and then the fluorescence intensities were measured. Moreover, for a specificity experiment, the nanosystem (16.4 μg/mL) was incubated with the complementary DNA targets for each MB and other cancer marker targets (MDR1-T, ETS1-T, SUR-T, GalNAc-T, c-myc-T, and TK1-T) for 0.5 h at 37 °C, while the DNA targets were 400 nM each. The fluorescence intensities of Quasar 670 and FAM were measured. The experiment was carried out at least three times for reducibility.

**Quantitation of Dox Loaded on GO.** (M + E)/Dox−GO (82 μg/mL GO) was added into the HEPES buffer (10 mM, pH 5.5) at 37 °C for 48 h. The mixture was centrifuged at 8000 rpm for 20 min, and the supernatant solution was applied for measuring the Dox's UV−vis absorbance. The Dox-loading capacity was calculated through $[(W_{Dox}/(W_{Dox} + W_{GO}) \times 100\%)]$, where $W_{Dox}$ and $W_{GO}$ are the weights of Dox and GO, respectively.

**Confocal Fluorescence Imaging.** MCF-7/Adr cells were seeded in confocal dishes and incubated for 24 h. PBS, (M + E)/Dox−GO (41 μg/mL), [(c-M + c-E)/Dox−GO) (41 μg/mL], (E/Dox−GO) (41 μg/mL), and (M/Dox−GO) (41 μg/mL) were incubated with MCF-7/Adr cells in RPMI-1640. After 6 h incubation, cells were washed twice with 1 mL of PBS and subjected to CLSM imaging with 488 nm excitation for Dox.

**Gene Expression Analysis by RT-PCR and Western Blot Analysis.** MCF-7/Adr cells were incubated with PBS, (c-M + c-E)/Dox−GO (41 μg/mL), MDR1/Dox−GO (M/Dox−GO) (41 μg/mL), ETS1/Dox−GO (E/Dox−GO) (41 μg/mL), and (M + E)/Dox−GO (41 μg/mL) nanosystem at 37 °C for 6 h. Afterward, RT-PCR and western blot analysis were performed 48 h later. Detailed steps are given in the Supporting Information.

**MTT Assay.** MTT assay was acquired to investigate the cytotoxicity of the nanosystem. MCF-7/Adr cells were planted into a 96-well plate and further cultured for 24 h. By removing the culture medium, cells were incubated with PBS, Dox (50.9 μM), (c-M + c-E)/Dox−GO (41 μg/mL), M/Dox−GO (41 μg/mL), E/Dox−GO (41 μg/mL), and (M + E)/Dox−GO (41 μg/mL) at 37 °C for 6 h. Then, the cells were replaced with 200 μL of fresh medium and further cultured for 48 h. The cells without any treatment as the control group were incubated for 48 h at 37 °C. Adding 200 μL MTT solution (0.5 mg/mL) to each well, the solution was removed after 4 h. To dissolve formazan formed by viable cells, 200 μL of DMSO was added to each well. The


DOI: 10.1021/acsami.8b02800
ACS Appl. Mater. Interfaces 2018, 10, 15461−15466

absorbance of formazan was measured at 490 nm with a microplate reader.

**Animal Studies.** All animal experiments were carried out by following the Principles of Laboratory Animal Care (People's Republic of China). Specific pathogen-free (SPF) female BALB/c nude mice were used in accordance with the guiding principles of the Animal Investigation Committee approved by Biology Institute of Shandong Academy of Science. Murine tumor xenograft models were generated by the subcutaneous injection of $1 \times 10^6$ MCF-7/Adr cells in PBS (150 $\mu$L) into the flank of female nude mice aged 4–6 weeks.

For gene silencing in vivo, when the tumor volume reached 50–100 $mm^3$, the mice ($n \geq 5$ per group) were divided into six groups: one with PBS (50 $\mu$L), while the other five groups were injected with Dox (101.8 $\mu$M, 50 $\mu$L), (c-M + c-E)/Dox–GO (820 $\mu$g/mL GO and 101.8 $\mu$M Dox, 50 $\mu$L), M/Dox–GO (820 $\mu$g/mL GO and 101.8 $\mu$M Dox, 50 $\mu$L), E/Dox–GO (820 $\mu$g/mL GO and 101.8 $\mu$M Dox, 50 $\mu$L), and (M + E)/Dox–GO (820 $\mu$g/mL GO and 101.8 $\mu$M Dox, 50 $\mu$L) three times at days 1, 3, and 5. The growing tumor volumes were measured with calipers every two days up to 14 days. The tumor volumes were calculated using the following equations: volume = (length × width$^2$)/2 and relative tumor volume = $V/V_0$ ($V_0$ is the original tumor volume). The monitored weights were also quite close. For histological analysis, mice were euthanized at the end of the treatments. Subsequently, tumors and major organs were harvested for routine staining with hematoxylin and eosin (H&E).

## RESULTS AND DISCUSSION

**Binding Studies of Dox and MB.** For Dox-loading capacity determination, a single MB Dox (1 $\mu$M) was incubated with different concentrations of MB and the fluorescence intensity of Dox was obtained later. The DNA sequences are displayed in Table S1. The phenolic, hydroxyl, and amino-sugar groups of Dox provide hydrogen bonding interactions with the double-stranded 5′-CG-3′ or 5′-GC-3′ sequences in the stem of the MB, and Dox's fluorescence was quenched via MBs, and its cytotoxicity got reduced as well.[24,25] The fluorescence intensities of Dox decreased with MB's increasing concentration till 500 nM (Figure S1), which represents the maximal fluorescence quenching of Dox. The fluorescence intensity of Dox revealed a slight change with the addition of more MBs (650 nM), indicating that two Dox molecules intercalate into one MB in accordance with the design of Scheme S1.

**Quantitation of GO.** For the next step, to estimate the optimized dosage of GO for the (M + E)/Dox–GO nanosystem, the fluorescence quenching capability of the prepared GO nanosheets was evaluated by mixing MDR1-Quasar 670 (250 nM) and ETS1-FAM (250 nM) with different concentrations of GO nanosheets. The fluorescence of Quasar 670 and FAM gradually declines with the growing concentration of GO nanosheets in Figure S2, until a complete quenching at the concentration of 82 $\mu$g/mL and no further fluorescence decrease were observed. Thus, 82 $\mu$g/mL of GO was chosen for the following experiments.

**Synthesis and Characterization of the (M + E)/Dox–GO Nanosystem.** The rings of Dox/MBs were attached to the hexagonal structure of the GO under the $\pi$-stacking interaction. To study the morphology and size distribution of GO and (M + E)/Dox–GO, HRTEM, DLS, AFM, and UV–vis were applied. In Figure 1a,b, the GO displays a sheet structure ~1.5 nm in thickness, and the (M + E)/Dox–GO nanosystem also demonstrates a sheet structure with a size of height profile ~4.5 nm (Figure S3). In Figure S4, (M + E)/Dox–GO has an intense absorption at ~260 and ~490 nm compared to GO, which associates with the typical absorption of MBs and Dox. Moreover, because Dox was effectively released from the GO

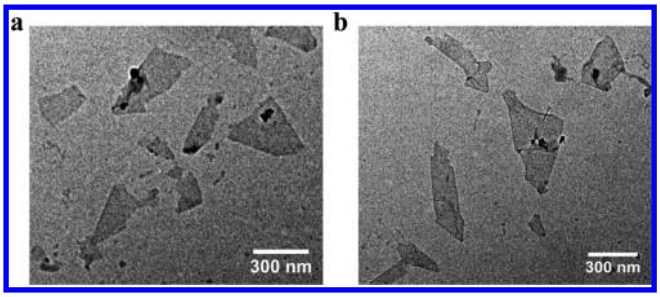


**Figure 1.** HRTEM images of (a) GO and (b) (M + E)/Dox–GO.

under endosomal pH (5.5),[26] the UV absorption exhibits the Dox-loading capacity that reached up to 35.25% (Figure S5). The results indicate that the nanosystem was successfully assembled, and the synthesis of the (M + E)/Dox–GO nanosystem has no influence on the appearance and dispersion of GO. In addition, DLS was also used to acquire the hydrodynamic diameter, and the average size of ~300 nm was obtained, indicating the same size range with HRTEM (Figure S6).

**Hybridization, Kinetic, and Specificity Experiments.** The hybridization experiments of MBs with the corresponding DNA targets were performed.[27] The fluorescence intensities of Quasar 670 and FAM were both enhanced with the rise of DNA target concentrations from 0 to 1000 nM (Figure 2a,b),

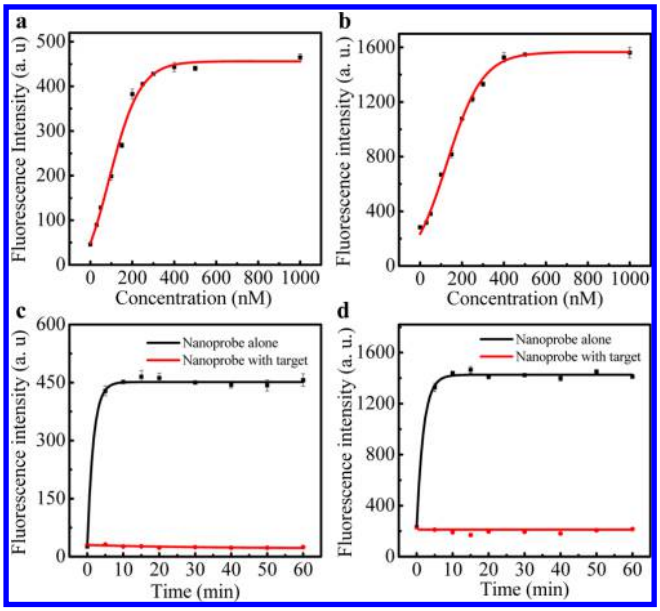


**Figure 2.** Fluorescence intensity profiles for the nanosystem (16.4 $\mu$g/mL) in the presence of various concentrations of (a) MDR1 target and (b) ETS1 target. The kinetic study of the nanosystem alone and with perfectly matched DNA targets (400 nM) of (c) MDR1 and (d) ETS1.

demonstrating that the fluorescence intensity is associated with the concentration of the DNA targets. Furthermore, the hybridization of the MBs and targets led to fluorescence recovery. To further evaluate the reaction kinetics, the fluorescence signals of the nanosystem with and without perfectly matched DNA targets were recorded. The nanosystem answered quickly to the corresponding DNA targets within 5 min (Figure 2c,d), suggesting a fast hybridization. Subsequently, the specificity of the nanosystem was explored in


DOI: 10.1021/acsami.8b02800
ACS Appl. Mater. Interfaces 2018, 10, 15461–15466

Figure S7, and it reveals that the nanosystem is remarkably specific and sensitive to a perfectly matched DNA targets and generated ~5 fold higher fluorescent signal intensities compared with other targets.

**The Stability of the Nanosystem.** The stability of (M + E)/Dox−GO was evaluated under physiological conditions to identify whether the MBs on GO can defend against enzymatic digestion.[28] The nanosystem treated with a common endonuclease, DNase I, exhibits quite slight fluorescence change compared to the case without DNase I in Figure S8. Nevertheless, the fluorescence intensities were all increased significantly after hybridization with the two perfectly matched DNA targets under the same conditions (Figure S8, inset). The results specify that the fluorescence increase is due to the hybridization of the nanosystem with targets, as well as its high nuclease stability. However, the mechanism of protection against enzymatic digestion is still not fully clear. It is assumed that the positively charged amine group of the nanocomposite repels $Mg^{2+}$, which is necessary for the enzymatic reaction. Moreover, the absorption of MBs on GO hinders the reaction of enzymes with the DNA, and GO efficiently protects MBs from enzymatic degradation.[29,30] These reasons limit the enzymatic cleavage.

**Downregulation of P-gp and Reversal of Dox Resistance.** To investigate the gene silencing efficacy of the (M + E)/Dox−GO nanosystem, the expression of MDR1 and ETS1 mRNAs in MCF-7/Adr cells by quantitative real-time polymerase chain reaction (RT-PCR) was evaluated. In Figure 3a, the mRNAs levels of MDR1 and ETS1 were remarkably

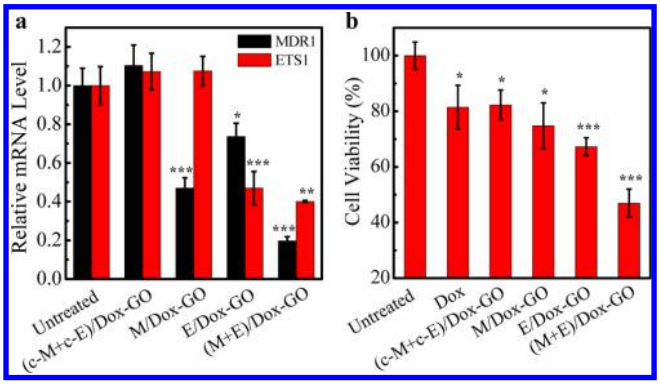


**Figure 3.** (a) PCR analysis of MDR1 and ETS1 expression in MCF-7/Adr cells under different treatments. (b) Cell viability of MCF-7/Adr cells treated with different samples for 48 h. Compared with the control groups, ***: $P < 0.001$; **: $P < 0.01$;*: $P < 0.05$.

downregulated by (M + E)/Dox−GO which resulted in 19.75 and 40.05% gene silencing rates, respectively. In addition, MDR1 mRNA expression in MCF-7/Adr cells treated with M/Dox−GO or E/Dox−GO was decreased to 46.98 or 73.71%. However, (c-M + c-E)/Dox−GO had no obvious influence on the expression of MDR1 and ETS1 mRNAs. The P-gp and ETS1 protein expressions were further studied using western blot analysis (Figure S9), and the inhibitory effect of the nanosystem on protein expression is consistent with RT-PCR. The results reveal that the (M + E)/Dox−GO nanosystem can downregulate P-gp expression in MCF-7/Adr cells, and ETS1 can upregulate the expression of MDR1. Furthermore, the relative silence ratio between the treatments without Dox and with Dox is ~1 (Figure S10). The results reveal that the mRNAs level of MDR1 and ETS1 after incubation with or without Dox was ignorable. Therefore, the (M + E)/Dox−GO nanosystem can be applied as an effective gene therapy agent for enhancing chemosensitivity of MCF-7/Adr cells to Dox.

To further evaluate the reversal of resistance to Dox in the MCF-7/Adr cells-induced (M + E)/Dox−GO nanosystem, intracellular accumulation of Dox was applied. In confocal fluorescence images (Figure 4a−f), the intracellular Dox

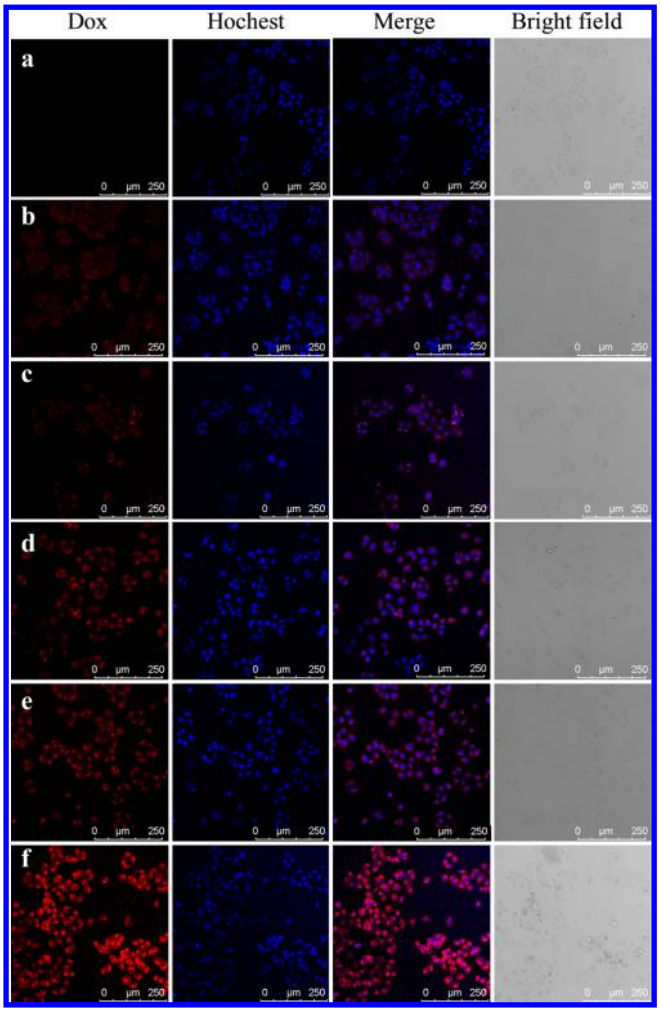


**Figure 4.** Confocal fluorescence images of intracellular Dox accumulation in MCF-7/Adr cells with treatment of (a) control, (b) Dox, (c) (c-M + c-E)/Dox−GO, (d) E/Dox−GO, (e) M/Dox−GO, and (f) (M + E)/Dox−GO.

concentration significantly accumulated in MCF-7/Adr cells treated with (M + E)/Dox−GO compared to PBS, Dox, (c-M + c-E)/Dox−GO, M/Dox−GO, and E/Dox−GO. It suggests that (M + E)/Dox−GO, M/Dox−GO, and E/Dox−GO mediation knocking down the P-gp can increase intratumor Dox accumulation and decrease Dox's efflux. In addition, the fluorescent signal of Dox gradually increased in an order of MCF-7/Adr cells incubated with PBS, Dox, (c-M + c-E)/Dox−GO, E/Dox−GO, M/Dox−GO, and (M + E)/Dox−GO.

Subsequently, the MCF-7/Adr cellular chemosensitivity toward Dox was also investigated through MTT assay.[31−33] Because the MTT dye can be reduced by the surviving cells to an insoluble formazan product in aqueous solutions, the amount of produced formazan can be determined spectrophotometrically once dissolved in dimethylsulfoxide. Therefore, the


DOI: 10.1021/acsami.8b02800
ACS Appl. Mater. Interfaces 2018, 10, 15461−15466

absorbance ratio of the treated/untreated cells represents their viability. Because of intracellular Dox accumulation, (M + E)/Dox−GO significantly raise their cytotoxicity to MCF-7/Adr cells. In Figure 3b, the viability of MCF-7/Adr cells treated with (M + E)/Dox−GO dramatically decreased compared to other samples under the same conditions. Moreover, the inhibition of MCF-7/Adr cells after incubation with the different concentration of GO was ignorable (Figure S11). These results confirm that the inhibition of P-gp results in an improved intracellular Dox concentration and apoptosis of MCF-7/Adr cells.

**In Vivo Inhibition of Tumor Growth.** To evaluate the in vivo therapeutic efficiency enhancement via P-gp knockdown by (M + E)/Dox−GO, the antitumor efficacy was performed in mice bearing MCF-7/Adr tumor. As the tumor volume reached 50−100 $mm^3$, the nude mice were randomly grouped into six groups ($n \geq 5$ for each group) and intratumorally injected with equivalent amounts of PBS (control group), Dox, (c-M + c-E)/Dox−GO, M/Dox−GO, E/Dox−GO, and (M + E)/Dox−GO. As shown in Figures 5a and S12, because of inhibiting the

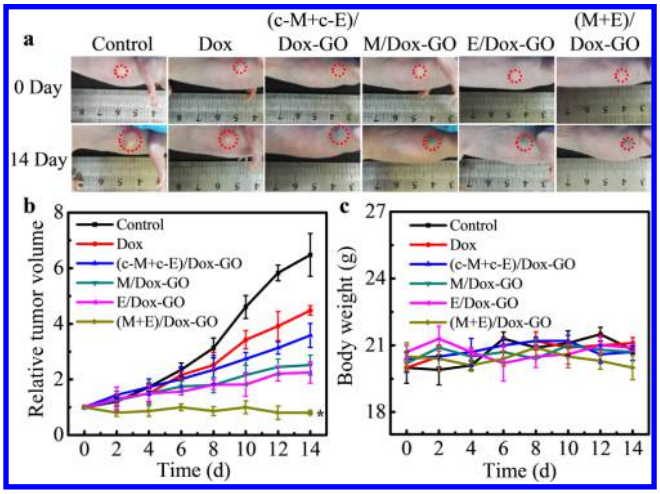


**Figure 5.** In vivo growth inhibition of the nanosystem in MCF-7/Adr tumors. (a) Photographs of the mice treated with PBS, Dox, (c-M + c-E)/-GO, M/Dox−GO, E/Dox−GO, and (M + E)/Dox−GO. (b) Tumor growth curves and (c) mice body weight. Compared with the control groups, *: $P < 0.05$.

expression of P-gp to enhance the effectiveness of chemotherapy, the tumor growth was inhibited in an order of mice treated with PBS (control group), Dox, (c-M + c-E)/Dox−GO, M/Dox−GO, E/Dox−GO, and (M + E)/Dox−GO. Moreover, the tumor volume was monitored during the animal studies (Figure 5b): the mice treated with (M + E)/Dox−GO stayed unchanged, whereas for the groups treated with PBS, Dox, (c-M + c-E)/Dox−GO, M/Dox−GO, and E/Dox−GO were found increasing at the end of the experiment by about 6.48, 4.48, 3.58, 2.52, and 2.25 folds. Meanwhile, no significant body weight fluctuation was observed through all groups (Figure 5c), implying that the treatments were free of severe systemic toxicity.

The antitumor efficiency of (M + E)/Dox−GO on tissue sections at 12 h after the treatments was further investigated via histopathological analysis. Hematoxylin and eosin (H&E)-stained tumor tissue revealed large-scale tissue damage in the (M + E)/Dox−GO group compared with the other groups (Figure 6). It implies that the (M + E)/Dox−GO has obvious

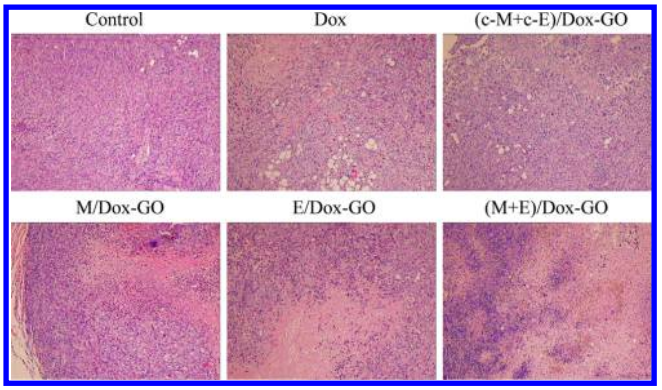


**Figure 6.** Histological analyses of H&E-stained tumor sections with different treatments.

toxicity toward tumor tissue. Additionally, histological examination of the major organs (heart, liver, spleen, lung, and kidney) confirmed no substantial tissue damage or inflammatory lesion in the 7 days after different treatments (Figure S13). The high antitumor effect and less systemic toxicity suggest that (M + E)/Dox−GO can potentially act as an ideal nanosystem for the reversal of Dox resistance.

## CONCLUSIONS

In summary, a novel drug-loaded nanosystem based on GO and MBs was successfully developed for reversing MDR in breast cancer. The nanosystem can release Dox by the acidic endosomes, as well as simultaneously silence the MDR1 gene and ETS1 gene by MBs hybridizing with target sequences. Additionally, it can effectively inhibit the expression of the Dox efflux transporter of P-gp and excellently restrain the development of MDR breast cancer. Compared to other MDR treatments, the strategy of multiple and multiplexed gene silencing combined with chemotherapy drugs is more economic and effective. Confocal fluorescence and flow cytometry data demonstrated that the Dox accumulation in breast cancer cells obviously increased. Furthermore, RT-PCR indicated that the expression of MDR1 mRNA treated with the synergistically silencing drug-loaded nanosystem (<20%) was much lower than that of the other control group (>45%). Animal studies further verified the better tumor inhibitory effect and little systematic toxicity. We expect that the treatment strategy can provide new routes for solving MDR problems in breast cancer and other cancers.

## ASSOCIATED CONTENT

### Supporting Information

The Supporting Information is available free of charge on the ACS Publications website at DOI: 10.1021/acsami.8b02800.

Binding affinity and nuclease stability, cell culture, gene expression, statistical analysis, AFM image and dynamic light scattering histograms of the nanosystems, standard linear calibration curves of Dox, the nuclease stability of the nanoprobe, specificity study, western blot, flow cytometry, and H&E staining images (PDF)

## AUTHOR INFORMATION

### Corresponding Authors

*E-mail: lina@sdnu.edu.cn (N.L.).
*E-mail: tangb@sdnu.edu.cn (B.T.)...



DOI: 10.1021/acsami.8b02800
ACS Appl. Mater. Interfaces 2018, 10, 15461−15466

**ORCID**

Bo Tang: 0000-0002-8712-7025

**Author Contributions**

†Y.L. and X.G. contributed equally to this work. The manuscript was written through contributions of all authors. All authors have given approval to the final version of the manuscript.

**Notes**

The authors declare no competing financial interest.

## ■ ACKNOWLEDGMENTS

This work was supported by National Natural Science Foundation of China (21390411, 21535004, 91753111, 21705098, and 21775094) and Natural Science Foundation of Shandong Province (JQ201503, ZR2015BQ003).

## ■ REFERENCES

(1) Gernaat, S. A. M.; Ho, P. J.; Rijnberg, N.; Lee, S. C.; Lim, S. H.; Yap, Y. S.; Grobbee, D. E.; Hartman, M.; Verkooijen, H. M. Risk of Death from Cardiovascular Disease Following Breast Cancer in Southeast Asia: A Prospective Cohort Study. *Sci. Rep.* **2017**, *7*, 1365−1371.

(2) Mitscher, L. A.; Pillai, S. P.; Gentry, E. J.; Shankel, D. M. Multiple Drug Resistance. *Med. Res. Rev.* **1999**, *19*, 477−496.

(3) Longley, D. B.; Johnston, P. G. Molecular Mechanisms of Drug Resistance. *J. Pathol.* **2005**, *205*, 275−292.

(4) Gottesman, M. M.; Fojo, T.; Bates, S. E. Multidrug Resistance in Cancer: Role of ATP-Dependent Transporters. *Nat. Rev. Cancer* **2002**, *2*, 48−58.

(5) Meng, H.; Liong, M.; Xia, T.; Li, Z.; Ji, Z.; Zink, J. I.; Nel, A. E. Engineered Design of Mesoporous Silica Nanoparticles to Deliver Doxorubicin and P-Glycoprotein siRNA to Overcome Drug Resistance in a Cancer Cell Line. *ACS Nano* **2010**, *4*, 4539−4550.

(6) Wu, J.; Wang, Y.-s.; Yang, X.-y.; Liu, Y.-y.; Yang, J.-r.; Yang, R.; Zhang, N. Graphene Oxide Used as a Carrier for Adriamycin can Reverse Drug Resistance in Breast Cancer Cells. *Nanotechnology* **2012**, *23*, 355101−355109.

(7) Wu, M.; Meng, Q.; Chen, Y.; Zhang, L.; Li, M.; Cai, X.; Li, Y.; Yu, P.; Zhang, L.; Shi, J. Large Pore-Sized Hollow Mesoporous Organosilica for Redox-Responsive Gene Delivery and Synergistic Cancer Chemotherapy. *Adv. Mater.* **2016**, *28*, 1963−1969.

(8) Xiong, X.-B.; Lavasanifar, A. Traceable Multifunctional Micellar Nanocarriers for Cancer-Targeted Co-delivery of MDR-1 siRNA and Doxorubicin. *ACS Nano* **2011**, *5*, 5202−5213.

(9) Wang, T.; Wang, D.; Yu, H.; Wang, M.; Liu, J.; Feng, B.; Zhou, F.; Yin, Q.; Zhang, Z.; Huang, Y.; Li, Y. Intracellularly Acid-Switchable Multifunctional Micelles for Combinational Photo/Chemotherapy of the Drug-Resistant Tumor. *ACS Nano* **2016**, *10*, 3496−3508.

(10) Yu, Z.; Pan, W.; Li, N.; Tang, B. A. Nuclear Targeted Dual-Photosensitizer for Drug-Resistant Cancer Therapy with NIR Activated Multiple ROS. *Chem. Sci.* **2016**, *7*, 4237−4244.

(11) Yuan, Y.; Wang, L.; Du, W.; Ding, Z.; Zhang, J.; Han, T.; An, L.; Zhang, H.; Liang, G. Intracellular Self-Assembly of Taxol Nanoparticles for Overcoming Multidrug Resistance. *Angew. Chem., Int. Ed.* **2015**, *127*, 9836−9840.

(12) Huang, P.-J. J.; Liu, J. Molecular Beacon Lighting up on Graphene Oxide. *Anal. Chem.* **2012**, *84*, 4192−4198.

(13) Luan, M.; Li, N.; Pan, W.; Yang, L.; Yu, Z.; Tang, B. Simultaneous Detection of Multiple Targets Involved in the PI3K/AKT Pathway for Investigating Cellular Migration and Invasion with a Multicolor Fluorescent Nanoprobe. *Chem. Commun.* **2017**, *53*, 356−359.

(14) Pan, W.; Zhang, T.; Yang, H.; Diao, W.; Li, N.; Tang, B. Multiplexed Detection and Imaging of Intracellular mRNAs Using a Four-Color Nanoprobe. *Anal. Chem.* **2013**, *85*, 10581−10588.

(15) Bao, C.; Conde, J.; Curtin, J.; Artzi, N.; Tian, F.; Cui, D. Bioresponsive antisense DNA gold nanobeacons as a hybrid in vivo theranostics platform for the inhibition of cancer cells and metastasis. *Sci. Rep.* **2015**, *5*, 12297−12309.

(16) Chen, T.; Wu, C. S.; Jimenez, E.; Zhu, Z.; Dajac, J. G.; You, M.; Han, D.; Zhang, X.; Tan, W. DNA Micelle Flares for Intracellular mRNA Imaging and Gene Therapy. *Angew. Chem., Int. Ed.* **2013**, *125*, 2066−2070.

(17) Conde, J.; Rosa, J.; de la Fuente, J. M.; Baptista, P. V. Gold-Nanobeacons for Simultaneous Gene Specific Silencing and Intracellular Tracking of the Silencing Events. *Biomaterials* **2013**, *34*, 2516−2523.

(18) Zhou, Q.; Ma, Y.; Wang, Z.; Wang, K.; Liu, R.; Han, Z.; Zhang, M.; Li, S.; Gu, Y. Optimized Ultrasound Conditions for Enhanced Sensitivity of Molecular Beacons in the Detection of MDR1 mRNA in Living Cells. *Anal. Chem.* **2016**, *88*, 2808−2816.

(19) Szakács, G.; Paterson, J. K.; Ludwig, J. A.; Booth-Genthe, C.; Gottesman, M. M. Targeting Multidrug Resistance in Cancer. *Nat. Rev. Drug Discovery* **2006**, *5*, 219−234.

(20) Buggy, Y.; Maguire, T. M.; McGreal, G.; McDermott, E.; Hill, A. D. K.; O'Higgins, N.; Duffy, M. J. Overexpression of the Ets-1 Transcription Factor in Human Breast Cancer. *Br. J. Cancer* **2004**, *91*, 1308−1315.

(21) Kars, M. D.; Işeri, Ö. D.; Gündüz, U. Drug Resistant Breast Cancer Cells Overexpress ETS1 Gene. *Biomed. Pharmacother.* **2010**, *64*, 458−462.

(22) Kato, T.; Fujita, Y.; Nakane, K.; Kojima, T.; Nozawa, Y.; Deguchi, T.; Ito, M. ETS1 Promotes Chemoresistance and Invasion of Paclitaxel-Resistant, Hormone-Refractory PC3 Prostate Cancer Cells by Up-Regulating MDR1 and MMP9 Expression. *Biochem. Biophys. Res. Commun.* **2012**, *417*, 966−971.

(23) Wei, J.; Zhou, Y.; Jiang, G.-Q.; Xiao, D. Silencing of ETS1 Reverses Adriamycin Resistance in MCF-7/ADR Cells via Down-regulation of MDR1. *Cancer Cell Int.* **2014**, *14*, 22−28.

(24) Fan, P.; Suri, A. K.; Fiala, R.; Live, D.; Patel, D. J. Molecular Recognition in the FMN-RNA Aptamer Complex. *J. Mol. Biol.* **1996**, *258*, 480−500.

(25) Pan, W.; Yang, H.; Zhang, T.; Li, Y.; Li, N.; Tang, B. Dual-Targeted Nanocarrier Based on Cell Surface Receptor and Intracellular mRNA: An Effective Strategy for Cancer Cell Imaging and Therapy. *Anal. Chem.* **2013**, *85*, 6930−6935.

(26) Huang, J.; Zong, C.; Shen, H.; Cao, Y.; Ren, B.; Zhang, Z. Tracking the intracellular drug release from graphene oxide using surface-enhanced Raman spectroscopy. *Nanoscale* **2013**, *5*, 10591−10598.

(27) Li, N.; Chang, C.; Pan, W.; Tang, B. A Multicolor Nanoprobe for Detection and Imaging of Tumor-Related mRNAs in Living Cells. *Angew. Chem., Int. Ed.* **2012**, *51*, 7426−7430.

(28) Gao, W.; Cao, W.; Sun, Y.; Wei, X.; Xu, K.; Zhang, H.; Tang, B. AuNP Flares-Capped Mesoporous Silica Nanoplatform for MTH1 Detection and Inhibition. *Biomaterials* **2015**, *69*, 212−221.

(29) He, X.-x.; Wang, K.; Tan, W.; Liu, B.; Lin, X.; He, C.; Li, D.; Huang, S.; Li, J. Bioconjugated Nanoparticles for DNA Protection from Cleavage. *J. Am. Chem. Soc.* **2003**, *125*, 7168−7169.

(30) Roy, I.; Ohulchanskyy, T. Y.; Bharali, D. J.; Pudavar, H. E.; Mistretta, R. A.; Kaur, N.; Prasad, P. N. Optical Tracking of Organically Modified Silica Nanoparticles as DNA Carriers: A Nonviral, Nanomedicine Approach for Gene Delivery. *Proc. Natl. Acad. Sci. U.S.A.* **2005**, *102*, 279−284.

(31) Li, N.; Li, Y.; Gao, X.; Yu, Z.; Pan, W.; Tang, B. Multiplexed Gene Silencing in Living Cells and in Vivo Using a DNAzymes-CoOOH Nanocomposite. *Chem. Commun.* **2017**, *53*, 4962−4965.

(32) Li, Y.; Li, N.; Pan, W.; Yu, Z.; Yang, L.; Tang, B. Hollow Mesoporous Silica Nanoparticles with Tunable Structures for Controlled Drug Delivery. *ACS Appl. Mater. Interfaces* **2017**, *9*, 2123−2129.

(33) Yu, Z.; Sun, Q.; Pan, W.; Li, N.; Tang, B. A Near-Infrared Triggered Nanophotosensitizer Inducing Domino Effect on Mitochondrial Reactive Oxygen Species Burst for Cancer Therapy. *ACS Nano* **2015**, *9*, 11064−11074.



DOI: 10.1021/acsami.8b02800
*ACS Appl. Mater. Interfaces* 2018, 10, 15461−15466